Heliyon 10 (2024) e27940

Contents lists available at ScienceDirect

Heliyon

journal homepage: www.cell.com/heliyon

Research article

Plasma metabolomic analysis reveals the metabolic characteristics and potential diagnostic biomarkers of spinal tuberculosis

Chaoran Wang [a,b], Caili Lou [b], Zongqiang Yang [a], Jiandang Shi [a], Ningkui Niu [a,c,*]

[a] Department of Orthopedics, General Hospital of Ningxia Medical University, Yinchuan 750004, Ningxia, China
[b] School of Clinical Medicine, Ningxia Medical University, Yinchuan 750004, Ningxia, China
[c] Research Center for Prevention and Control of Bone and Joint Tuberculosis, General Hospital of Ningxia Medical University, Yinchuan 750004, Ningxia, China

ARTICLE INFO

Keywords:
Spinal tuberculosis
Metabolomics
Diagnostic biomarkers
Pathogenesis

ABSTRACT

Objectives: This study aimed to conduct a non-targeted metabolomic analysis of plasma from patients with spinal tuberculosis (STB) to systematically elucidate the metabolomic alterations associated with STB, and explore potential diagnostic biomarkers for STB.

Methods: From January 2020 to January 2022, 30 patients with spinal tuberculosis (STBs) clinically diagnosed at the General Hospital of Ningxia Medical University and 30 age- and sex-matched healthy controls (HCs) were selected for this study. Using ultra-high performance liquid chromatography coupled with quadrupole time-of-flight mass spectrometry (UPLC-QTOF/MS) based metabolomics, we analyzed the metabolic profiles of 60 plasma samples. Statistical analyses, pathway enrichment, and receiver operating characteristic (ROC) analyses were performed to screen and evaluate potential diagnostic biomarkers.

Results: Metabolomic profiling revealed distinct alterations between the STBs and HCs cohorts. A total of 1635 differential metabolites were screened, functionally clustered, and annotated. The results showed that the differential metabolites were enriched in sphingolipid metabolism, tuberculosis, cutin, suberine and wax biosynthesis, beta-alanine metabolism, methane metabolism, and other pathways. Through the random forest algorithm, LysoPE (18:1(11Z)/0:0), 8-Demethyl-8-formylriboflavin 5′-phosphate, Glutaminyl-Gamma-glutamate, (2R)-*O*-Phospho-3-sulfolactate, and LysoPE (P-16:0/0:0) were determined to have high independent diagnostic value.

Conclusions: STBs exhibited significantly altered metabolite profiles compared with HCs. Here, we provide a global metabolomic profile and identify potential diagnostic biomarkers of STB. Five potential independent diagnostic biomarkers with high diagnostic value were screened. This study provides novel insights into the pathogenesis, diagnosis, and treatment strategies of STB.

1. Introduction

Spinal tuberculosis (STB), an extrapulmonary manifestation of tuberculosis (TB) caused by *Mycobacterium tuberculosis* (*MTB*), is the most common form of osteoarticular TB, accounting for over 60% of all cases [1,2]. It is associated with multiple RNAs, involves

* Corresponding author. Department of Orthopedics, General Hospital of Ningxia Medical University, 804 Shengli South Street, Xingqing District, Yinchuan 750004, Ningxia, China
E-mail address: niuningkui6743242@163.com (N. Niu).

https://doi.org/10.1016/j.heliyon.2024.e27940
Received 10 March 2023; Received in revised form 16 February 2024; Accepted 8 March 2024
Available online 22 March 2024

multiple signaling pathways, and has a complex pathogenesis [3–5]. The onset of STB is slow. Patients present with back pain with or without systemic symptoms, often accompanied by a series of severe clinical symptoms, such as kyphotic deformity and/or neurological complications at the time of consultation. Existing techniques have several limitations in the diagnosis of STB [6]. Culture and serological tests have low positivity rates and are time-consuming; imaging tests such as digital radiography (DR), computed tomography (CT), and magnetic resonance imaging (MRI) lack specificity; and the use of molecular tests such as Xpert *Mycobacterium tuberculosis* complex and resistance to rifampin (Xpert *MTB*/RIF) and whole-genome sequencing (WGS) is limited by high costs and complex instrumentation [7–9]. In recent years, nucleic acid amplification test (NAAT) has been further developed and applied, and the diagnostic efficacy of this technology continues to be reported [10,11]. In conclusion, due to insufficient awareness of the disease, the rates of underdiagnosis and delayed diagnosis are high, posing a significant threat to the health of patients [12]. Therefore, further investigation into the pathogenesis of STB and research into effective diagnostic methods are urgently needed [13].

In clinical practice, detecting biomarkers in the plasma is a useful auxiliary method for diagnosing diseases [14]. Metabolomics is an emerging "omics" method that can be used to comprehensively analyze the changes of endogenous and exogenous compounds and systematically study the final metabolites produced by genetic and protein changes during the adjustment of organisms after external stimuli [15]. This method has been widely used to elucidate pathogenesis, diagnose diseases, and predict prognosis [16]. However, few metabolomic studies have been conducted on STB [17].

In the present study, we analyzed metabolites in the plasma of patients with spinal tuberculosis (STBs) and age- and sex-matched healthy controls (HCs) using ultra-high performance liquid chromatography coupled with quadrupole time-of-flight mass spectrometry (UPLC-QTOF/MS). The aim was to systematically reveal metabolic changes in STB disease states and select the most discriminative biomarkers to provide a reliable basis for the pathogenesis, diagnosis, and treatment strategies of STB.

2. Materials and methods

2.1. Diagnostic criteria for STB

From January 2020 to January 2022, patients who met the following criteria were diagnosed with STB in the General Hospital of Ningxia Medical University: (1) history of contact with TB; (2) symptoms of TB intoxication, such as low-grade fever, night sweats, weakness, and wasting; (3) pain at the lesion site, pressure and percussion pain at the spinous processes or paraspinal processes, and radiating pain at the innervated area of the lesion; (4) muscle spasms and decreased range of motion; (5) change in physiologic curvature of the spine and appearance of posterior convexity deformity; (6) appearance of abscess or sinus tract at the lesion site; (7) neurologic dysfunction; (8) positive smear, culture, serologic tests, molecular tests, erythrocyte sedimentation rate (ESR), and C-reactive protein (CRP); (9) radiographic evidence such as DR, CT, and MRI showing STB.

2.2. Inclusion and exclusion criteria for STBs

Inclusion criteria: (1) diagnosed with STB based on the above criteria; (2) underwent surgical treatment and were confirmed by postoperative histopathology to have STB caused by *MTB* infection; (3) with complete medical history and data.

Exclusion criteria: (1) pregnant or lactating women; (2) with trauma, tumor, TB in other parts, other infectious diseases, immunodeficiency diseases, metabolic diseases and other diseases that cause metabolic changes; (3) received standard anti-TB drugs for more than seven days; (4) used hormones and other drugs within three months.

2.3. Inclusion and exclusion criteria for HCs

HCs were recruited from the physical examination center during the same period.

Inclusion criteria: (1) age- and sex-matched healthy individuals; (2) no history of TB; (3) with complete medical history and data.

Exclusion criteria: (1) pregnant or lactating women; (2) used antibiotics, hormones, and other drugs within three months.

2.4. Evaluation of clinical characteristics and multiple markers

Simultaneously, peripheral blood samples were collected, and the relevant clinical information of each participant was recorded individually with corresponding numbers to establish a unified and complete paper and electronic case database.

The demographics, inflammatory indicators (white blood cell count [WBC] and lymphocyte [Lymph%], neutrophil [Neut%], monocyte [Mono%], eosinophil [Eos%], and basophil [Baso%] percentages), digestive system indicators (aspartate aminotransferase [AST], alanine aminotransferase [ALT], aspartate aminotransferase/alanine aminotransferase [AST/ALT], total protein [TP], albumin [Alb], globulin [Glo], and albumin/globulin [A/G]), hematological indicators (red blood cell count [RBC] and hemoglobin [Hb]), urinary system indicators (serum creatinine [Scr] and serum urea [Sur]), and other indicators (fasting blood glucose [FBG] and uric acid [UA]) were analyzed and compared.

This study was approved by the Medical Research Ethics Review Committee of General Hospital of Ningxia Medical University, and all participants provided written informed consent to participate in the study. All research methods and experimental protocols in this study were established in accordance with the ethical guidelines of the Declaration of Helsinki and relevant regulations.

2.5. Samples' collection, storage, and pretreatment

All peripheral blood samples were collected aseptically in the morning after fasting. The day of collection was the seventh day of anti-TB treatment, and all patients had not taken any medication for 24 h prior to collection. Three days before collection, the study participants were instructed to consume a light diet, and after 8 p.m. on the day before collection, the study participants were instructed to fast, abstain from drinking water, and rest on time. For each participant, 5 ml of venous blood was collected from the elbow using a heparin-sodium anticoagulation tube. After mixing the blood and additives, two-step centrifugation was performed to remove blood cells, cell debris, and precipitated particles from the sample solution. Transfer the plasma samples into Eppendorf (EP) tubes using a pipette. Label the tube with the sample information and immediately freeze at −80 °C.

The pretreatment procedure for all samples was as follows. Samples (100 μL) were measured, 500 μL of extraction solvent (methanol to acetonitrile solution, volume ratio = 1:1) containing the internal standard (2-Chloro-L-phenylalanine, 20 mg/L) was added, then the mixture was vortexed for 30 s, sonicated for 10 min (in an ice water bath), stored at −20 °C for 1 h, and centrifuged at 4 °C for 15 min at 12,000 rpm. Then, 500 μL of the supernatant was placed in an EP tube and dried in a vacuum concentrator. Next, 160 μL of acetonitrile to water solution (volume ratio = 1:1) was added to the extract for re-dissolution, then vortexed for 30 s, and sonicate for 10 min (in an ice water bath). The samples were then centrifuged at 4 °C for 15 min at 12,000 rpm. The supernatant (120 μL) was carefully inserted in a 2 mL liquid chromatography vial. Ten μL of each sample was mixed into quality control samples (QCs) and tested in the same processing method as the 60 formal samples to monitor the stability of the UPLC-QTOF/MS system [18].

2.6. Metabolites extraction

The UPLC-QTOF/MS system for metabolomic analysis was composed of a Waters ACQUITY I-Class PLUS ultra-high performance liquid chromatography (UPLC) tandem Waters Xevo G2-XS QTOF high-resolution mass spectrometer. The ACQUITY UPLC HSS T3 column (1.8 μm, 2.1 mm*100 mm) was purchased from Waters. Positive ion mode: mobile phase A, 0.1% aqueous formic acid solution; mobile phase B, 0.1% acetonitrile formic acid solution. Negative ion mode: mobile phase A, 0.1% aqueous formic acid solution; mobile phase B, 0.1% acetonitrile formic acid solution. The injection volume was 1 μL [19].

2.7. UPLC-QTOF/MS analysis

A Waters Xevo G2-XS QTOF high-resolution mass spectrometer was used to collect primary and secondary mass spectrometry data in MSe mode with acquisition software (Mass Lynx V4.2, Waters). In each data acquisition cycle, dual-channel data acquisition was performed simultaneously at both low and high collision energies. The low collision energy was 2 V, the high collision energy range was 10–40 V, and the scanning frequency was 0.2 s for the mass spectrum. The parameters of the electron spray ionization (ESI) ion source are as follows: capillary voltage: 2000 V (positive ion mode) or −1500 V (negative ion mode), cone voltage: 30 V, ion source temperature: 150 °C, desolvation gas temperature: 500 °C, backflush gas flow rate: 50 L/h, and desolvation gas flow rate: 800 L/h [19].

2.8. Data preprocessing and annotation

The raw data collected using Mass Lynx V4.2 were processed using Progenesis QI software for peak extraction, peak alignment, and other data processing operations based on the Progenesis QI software online METLIN database, public database, and Biomark's self-built library for identification. Theoretical fragment identification was performed simultaneously, and the mass deviation of the parent ion was 100 ppm and that of the fragment ion was 50 ppm [19]. After the data search was completed, the overall quality of the data was evaluated, principal component analysis (PCA) was performed, and PCA plots were generated to determine the repeatability of the samples within the group and the stability of the samples' biological duplication.

2.9. Statistical analysis

2.9.1. Statistical analysis of clinical data

For clinical data, continuous variables were expressed as mean ± standard deviation (SD). The chi-squared test was used to compare categorical variables, the Shapiro-Wilk test was used to detect the normality of continuous variables, and two independent samples *t*-test or Mann-Whitney U tests were used to compare normal or partial normal continuous variables, respectively. Statistical analysis was performed using IBM SPSS Statistics 26 software and R software. Statistical significance was set at $P < 0.05$.

2.9.2. Statistical analysis of metabolomics

For metabolomic data, after normalizing the original peak area information with the total peak area, a follow-up analysis was performed. PCA and Spearman's correlation analysis were used to evaluate the repeatability of samples from STBs, HCs, and QCs. The identified compounds were searched for classification and pathway information using the Kyoto Encyclopedia of Genes and Genomes (KEGG), Human Metabolome Database (HMDB), and Lipid Metabolites and Pathways Strategy (LIPID MAPS). The fold change (FC) between STBs and HCs was calculated and compared, and the significance of the difference for each compound was calculated using univariate statistical analysis methods. The *t*-test was used when the normality test indicated that the data followed a normal distribution, and the nonparametric Wilcoxon test was used when the normal distribution was not satisfied. The R language package ropls was used to perform orthogonal projections to latent structures discriminant analysis (OPLS-DA) modeling, and 200 permutation tests

were performed to verify the reliability of the model. The variable importance in projection (VIP) value of the model was calculated using multiple cross-validations. The method of combining the FC, *P*-value, and VIP value of the OPLS-DA model was adopted to screen for differential metabolites. The screening criteria were $|FC| \geq 1$, $P < 0.05$, and VIP ≥ 1. Enrichment analysis of KEGG annotation results of differential metabolites was conducted using the R language package cluster profiler and hypergeometric test.

3. Results

3.1. Clinical characteristics of enrolled subjects

In this study, 60 participants were recruited, including 30 STBs (n = 30) and 30 HCs (n = 30), their overall baseline characteristics are shown in Table 1. The STBs and HCs were matched for gender and age, with no statistical differences ($P > 0.05$). Compared with HCs, STBs exhibited higher levels of Neut%, Mono%, AST/ALT, Glo, and FBG, and lower levels of Lymph%, Eos%, Alb, A/G, and Hb ($P < 0.05$).

3.2. Quality control and overall metabolic characteristics

The Pearson or Spearman correlation coefficients of the metabolite content of the QCs were calculated to show the correlation between the QCs. The results showed that the minimum correlation value of the QCs in this study was >0.75, and the percentage of peaks with relative standard deviation (RSD) ≤ 30% in the total number of identified peaks was ≥0.6 (Table S1). The above results indicate that the reproducibility of the QCs and the stability of the instrument in this study were satisfactory.

Qualitative and quantitative metabolomic analyses were performed on 60 samples, and 16,000 peaks were detected, with a total of 4755 metabolites were annotated, as shown in Table S2. To elucidate the overall metabolic differences between the groups and the variability between samples within the groups, we performed PCA and generated a PCA plot including the STBs, HCs, and QCs, as shown in Fig. 1A. The results showed that the QCs (green) clustered tightly, indicating instrument stability. In addition, three outlier samples shown in the HCs numbered A7, A10, and A21, were excluded from further analysis, whereas the remaining samples showed good intra-group reproducibility and inter-group variability. The PCA plot, after excluding the three outlier samples, is shown in Fig. 1B.

To demonstrate the differences between STBs and HCs, discriminant analysis was performed on the metabolic data of the two groups by establishing an OPLS-DA model. After seven cross-validations of the model, the results showed large R^2Y and Q^2Y values ($R^2Y = 0.946$, $Q^2Y = 0.829$), indicating that the established OPLS-DA model was stable and reliable with good adaptability and predictability, and can be used for subsequent differential metabolite searches and analyses (Fig. 1C). To further verify the reliability of the OPLS-DA model, a permutation test was performed, and the results were satisfactory, as shown in Fig. 1D.

The identified compounds were searched for classification and pathway information in KEGG, HMDB, and LIPID MAPS; the most

Table 1
Clinical characteristics of the enrolled STB patients (STBs) and matched healthy controls (HCs).

	Reference interval	HCs	STBs	*P*-value
Sample size	N/A	30	30	N/A
Gender (male/female)	N/A	16/14	14/16	0.606[#]
Age (years)	N/A	42.60 ± 12.00	46.20 ± 15.80	0.326[*]
White blood cell count, WBC (10^9/L)	3.50–9.50	5.95 ± 0.87	6.23 ± 1.30	0.107[*]
Lymphocyte percent, Lymph% (%)	20.00–50.00	34.42 ± 4.20	31.16 ± 8.23	0.003[*a]
Neutrophil percent, Neut% (%)	40.00–75.00	56.55 ± 4.79	59.72 ± 8.56	0.005[*a]
Monocyte percent, Mono% (%)	3.00–10.00	6.53 ± 1.18	6.93 ± 1.72	0.008[**a]
Eosinophil percent, Eos% (%)	0.40–8.00	2.00 ± 1.56	1.72 ± 1.39	0.040[**a]
Basophil, Baso% (%)	0.00–1.00	0.63 ± 0.57	0.57 ± 0.49	0.115[**]
Aspartate aminotransferase, AST (U/L)	13.00–35.00	18.62 ± 6.01	20.52 ± 10.85	0.288[**]
Alanine aminotransferase, ALT (U/L)	7.00–40.00	21.51 ± 9.63	21.13 ± 10.56	0.417[**]
Aspartate aminotransferase/Alanine aminotransferase, AST/ALT	0.00–1.00	0.94 ± 0.26	1.07 ± 0.43	0.019[*a]
Total protein, TP (g/L)	65.00–85.00	72.53 ± 13.82	72.24 ± 12.12	0.092[**]
Albumin, Alb (g/L)	40.00–55.00	48.33 ± 5.80	45.30 ± 7.44	0.000[**a]
Globulin, Glo (g/L)	20.00–40.00	28.26 ± 3.90	30.09 ± 5.89	0.003[**a]
Albumin/Globulin, A/G	1.20–2.40	2.71 ± 5.38	2.27 ± 4.59	0.000[**a]
Red blood cell count, RBC (10^{12}/L)	3.80–5.10	4.79 ± 0.63	4.74 ± 0.65	0.352[**]
Hemoglobin, Hb (g/L)	115.00–150.00	144.61 ± 21.91	140.43 ± 22.18	0.014[**a]
Serum creatinine, Scr (μmol/L)	41.00–73.00	61.27 ± 14.97	59.13 ± 14.62	0.136[*]
Serum urea, Sur (mmol/L)	2.60–7.50	5.08 ± 0.99	5.03 ± 1.04	0.654[*]
Fasting blood glucose, FBG (mmol/L)	3.90–6.10	4.60 ± 0.45	4.84 ± 1.36	0.045[**a]
Uric acid, UA (μmol/L)	155.00–357.00	357.30 ± 106.13	350.36 ± 110.30	0.526[*]

N/A = Not Applicable.
[a] with statistical significance.
[#] By Chi-squared test.
[*] By Two independent samples *t*-test.
[**] By Mann-Whitney *U* test.

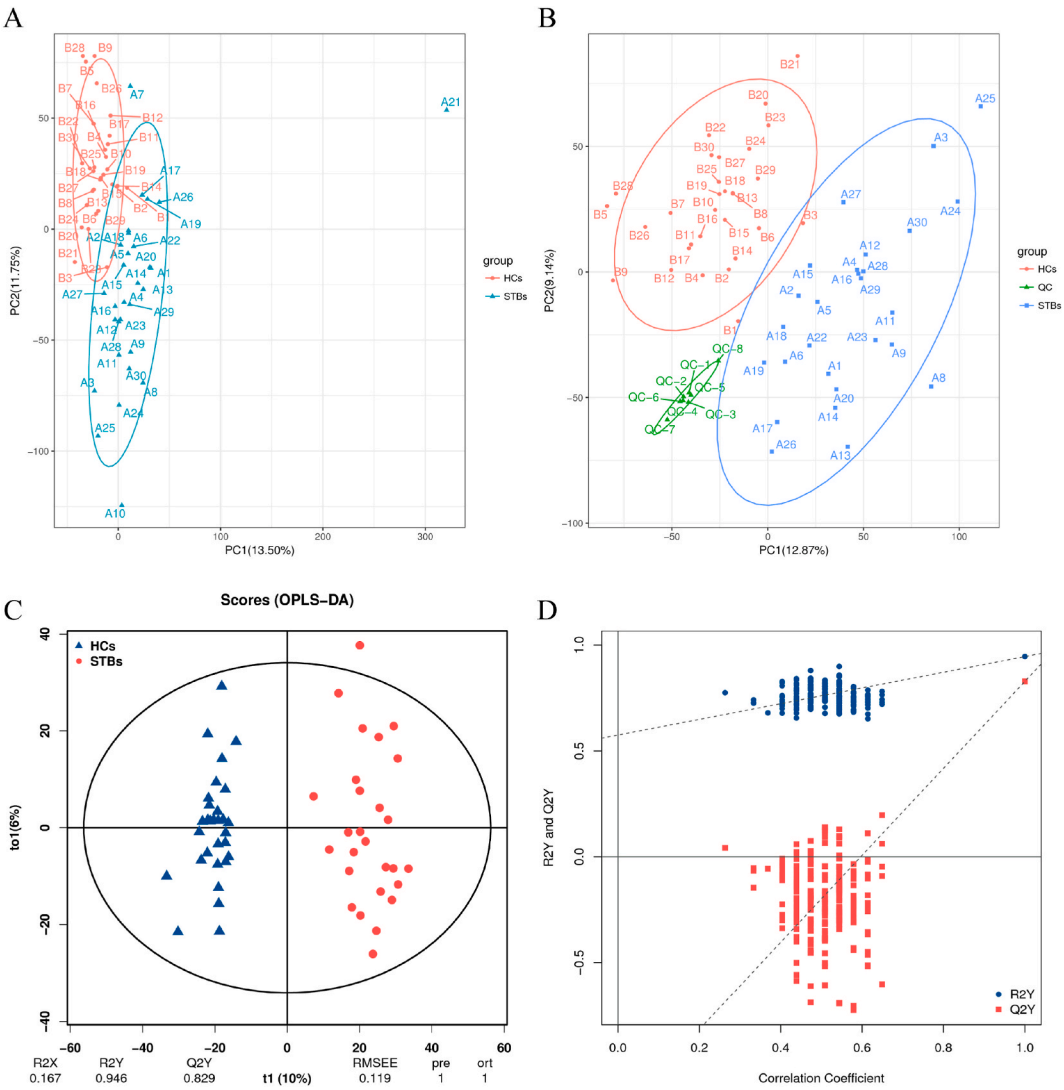

Fig. 1. Quality control and overall metabolic characteristics: (A) PCA plot of all samples from STBs, HCs, and QCs; (B) PCA plot for STBs, HCs, and QCs after excluding three outlier samples; (C) OPLS-DA score plot for STBs and HCs; (D) OPLS-DA model replacement test plot for STBs and HCs.

annotated metabolite species in each database were chemical structure transformation maps, lipids and lipid-like molecules, and fatty acyls. The top 20 species with the most annotation information in each database were selected, and a summary bar chart and annotation table were generated, as shown in Fig. 2B–D.

3.3. *Differential metabolic profiles between STBs and HCs*

Through the screening criteria ($|FC| \geq 1$, $P < 0.05$, and VIP ≥ 1), 1635 differential metabolites were screened between STBs and HCs, of which 863 metabolites were increased and 772 metabolites were decreased in STBs compared to HCs, as shown in Table S3. To visualize the overall trend and statistical significance of the differential metabolite content in the two groups, a volcano plot was drawn, as shown in Fig. 2A. A random forest analysis was performed to estimate the importance of each metabolite (500 decision trees). As shown in Fig. 3A and Table S4, five metabolites showed the highest independent diagnostic values, including LysoPE (18:1 (11Z)/0:0), 8-Demethyl-8-formylriboflavin 5′-phosphate, Glutaminyl-Gamma-glutamate, (2R)-*O*-Phospho-3-sulfolactate, and LysoPE (P-16:0/0:0).

3.4. *Reliability of potential diagnostic biomarkers*

The area under the curve (AUC) values of LysoPE (18:1(11Z)/0:0), 8-Demethyl-8-formylriboflavin 5′-phosphate, Glutaminyl-Gamma-glutamate, (2R)-*O*-Phospho-3-sulfolactate, and LysoPE (P-16:0/0:0) were 0.996, 0.986, 0.969, 0.990, and 0.935

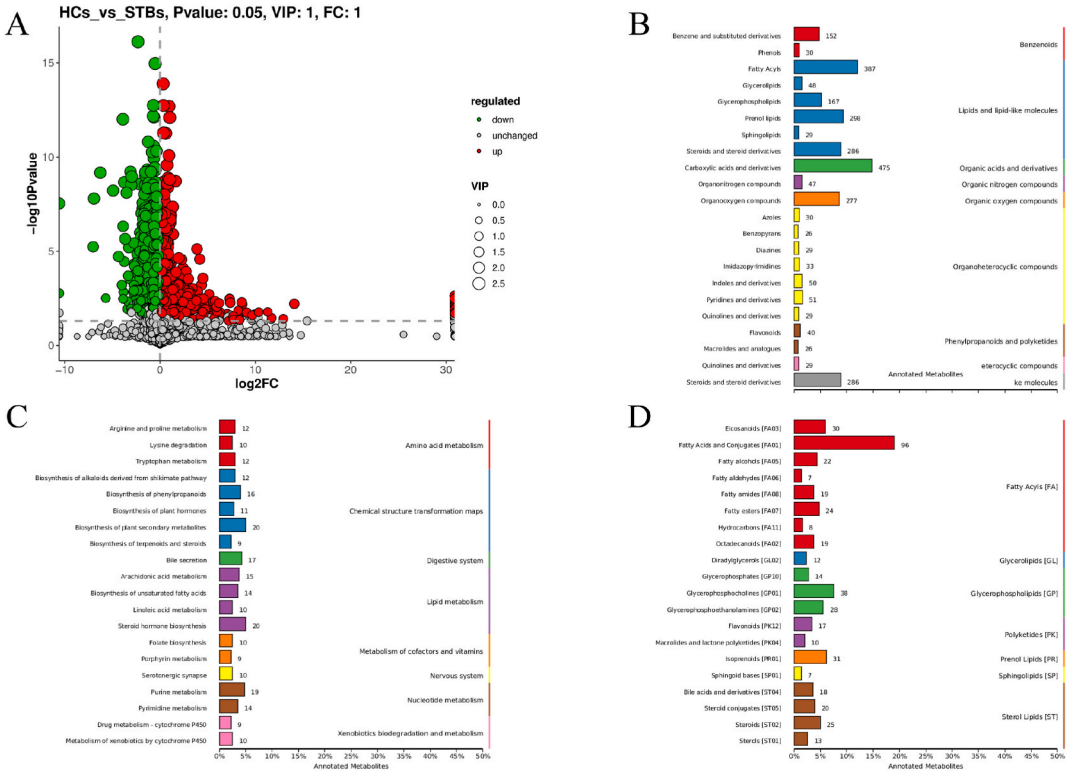

Fig. 2. Identification of differentially expressed metabolites between STBs and HCs: (A) volcano plot from untargeted metabolomics analysis showing increased (red) or decreased (green) plasma metabolites of STBs compared to HCs; (B) summary bar chart and annotation table of all identified metabolites in the HMBD database; (C) summary bar chart and annotation table of all identified metabolites in the KEGG database; (D) summary bar chart and annotation table of all identified metabolites in the LIPID MAPS database. (For interpretation of the references to colour in this figure legend, the reader is referred to the Web version of this article.)

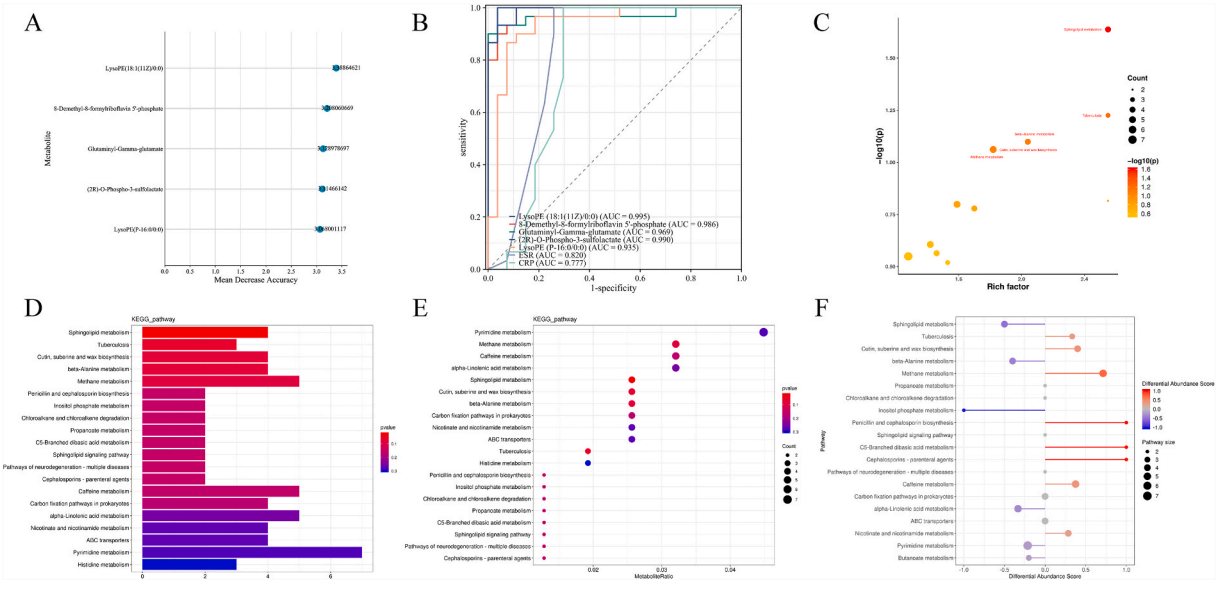

Fig. 3. Random forest analysis, KEGG function annotation, and enrichment analysis of differentially expressed metabolites: (A) mean decrease accuracy plot obtained from random forest analysis of differential metabolites; (B) ROC curve for five potential diagnostic biomarkers; (C) bubble map of KEGG enrichment factors for differential metabolites; (D) pathway enrichment classification map for differential metabolites; (E) scatter plot of KEGG enrichment for differential metabolites; (F) differential abundance score plot showing the direction of content change for all annotated differential metabolites.

respectively. As shown in Table 2, Table S5, and Fig. 3B.

3.5. Correlation between five potential diagnostic biomarkers and clinical indicators

Correlation analysis revealed correlations between five potential diagnostic biomarkers and several clinical indicators, as shown in and Table S6 and Fig. 4A–E. Among them, Alb was correlated with all five potential diagnostic biomarkers, with positive correlations with LysoPE (18:1(11Z)/0:0), Glutaminyl-Gamma-glutamate, and LysoPE (P-16:0/0:0), and negative correlations with 8-Demethyl-8-formylriboflavin 5′-phosphate and (2R)-*O*-Phospho-3-sulfolactate.

3.6. KEGG function annotation and enrichment analysis

Enrichment analysis of KEGG annotation results of differential metabolites using cluster profiler with hypergeometric test showed that the differential metabolites were enriched in sphingolipid metabolism, tuberculosis, cutin, suberine and wax biosynthesis, beta-alanine metabolism, methane metabolism, and other pathways (Fig. 3C–E).

The differential abundance score plot (Fig. 3F) shows the average and overall changes of all metabolites in each pathway. All annotated metabolites in penicillin and cephalosporin biosynthesis, C5-branched dibasic acid metabolism, and cephalosporins-parenteral agents pathways increased, and all annotated metabolites in inositol phosphate metabolism pathways increased.

4. Discussion

TB infection may alter the levels of RNA, proteins, and metabolites [20,21], our previous study determined that the expression of lipopolysaccharide-binding protein (LBP) in the peripheral blood was significantly higher in patients with STB than in the normal population [22]. Based on the central dogma of molecular biology [23], metabolites as downstream products of proteins may be able to distinguish STBs from HCs and elucidate the pathogenesis of STB infection. Metabolomics has been widely used as a stable and high-throughput method for several infectious and non-infectious diseases, and the establishment of peripheral blood metabolic biomarkers using this method is important for the diagnosis and study of pathogenesis. However, little information is available regarding the metabolomics of STB [24].

Therefore, in this study, UPLC-QTOF/MS was used to perform high-throughput detection of changes in the host plasma metabolome caused by *MTB* infection. Our metabolomic profiling results showed significant differences between the STBs and HCs cohorts. Enrichment analysis of KEGG annotation results for differential metabolites showed that STB was mainly related to pathways such as sphingolipid metabolism. Due to the extensive and high-dimensional nature of metabolomics, we used random forest analysis to select potential independent diagnostic biomarkers that were differentially expressed between the two groups: LysoPE (18:1(11Z)/0:0), 8-Demethyl-8-formylriboflavin 5′-phosphate, Glutaminyl-Gamma-glutamate, (2R)-*O*-Phospho-3-sulfolactate, and LysoPE (P-16:0/0:0).

LysoPE (18:1(11Z)/0:0) and LysoPE (P-16:0/0:0) are lysophosphatidylethanolamine (LPE), a type of lysophospholipids (LPLs). LPLs are intermediates of various phospholipid synthesis pathways, which are the major components of biological membranes, and are important signaling mediators with a wide range of biological effects that affect various processes such as carcinogenesis, neurogenesis, and immunity [25]. LPE accumulates in human serum and can reach concentrations of several hundred nanograms per milliliter [26]; however, little research has been conducted on its effects. Studies have shown that LPE induces intracellular calcium mobilization, chemotactic migration, and cellular invasion through G-protein-coupled receptors (GPCRs) through two different methods [27,28], and inhibits serum deprivation-induced apoptosis, induces neuronal differentiation in cultured PC-12 cells through the mitogen-activated protein kinases (MAPK) signal cascade [29], and increases intracellular Ca^{2+} levels through the LPA1/Gi/o proteins/phospholipase C/IP3/Ca^{2+} rise/Ca^{2+} influx pathway in PC-12 neuronal cells [30]. In addition, 2-polyunsaturated acyl-LPE diminishes the formation of leukotriene C_4 (LTC_4), a lipid mediator responsible for vascular permeability, and diminishes the formation of leukotriene B_4 (LTB_4) and 12-HETE, which are potent chemotactic factors. The levels of pro-inflammatory mediators (IL-1β, IL-6, TNF-α, or NO) were reduced, whereas the level of anti-inflammatory interleukin IL-10 was increased with LPE induction [31].

Studies have shown that plasma IL-6 and LTB_4 levels are significantly elevated in patients with TB [32], and that these levels are highest among patients in advanced stages [33], and decrease after treatment [34]. The level of plasma 12-HETE is elevated [35] and high levels of LTB_4 lead to TNF-α overproduction, macrophage necrosis, and enhanced growth of *MTB* [36]. Inactivation of inflammatory mediator LTB_4 by related enzymes inhibits *MTB* infection [37]. In addition, the elimination of lipid accumulation in

Table 2
Diagnostic performance of screened potential diagnostic biomarkers.

	Sensitivity	Specificity	Accuracy	AUC (95%*CI*)
LysoPE (18:1(11Z)/0:0)	1.000	0.963	0.982	0.995(0.984–1.000)
8-Demethyl-8-formylriboflavin 5′-phosphate	1.000	0.889	0.947	0.986(0.966–1.000)
Glutaminyl-Gamma-glutamate	0.900	1.000	0.947	0.969(0.919–1.000)
(2R)-*O*-Phospho-3-sulfolactate	0.933	0.963	0.947	0.990(0.975–1.000)
LysoPE (P-16:0/0:0)	0.867	0.926	0.895	0.935(0.864–1.000)
ESR	1.000	0.741	0.877	0.820(0.690–0.949)
CRP	1.000	0.704	0.860	0.777(0.633–0.920)

CI = Confidence Interval.

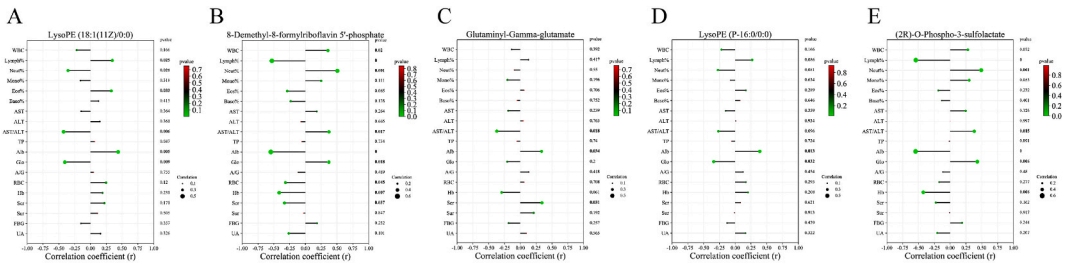

Fig. 4. Correlation of five potential diagnostic biomarkers with clinical indicators: (A) correlation between LysoPE (18:1(11Z)/0:0) and clinical indicators; (B) correlation between 8-Demethyl-8-formylriboflavin 5′-phosphate and clinical indicators; (C) correlation between Glutaminyl-Gamma-glutamate and clinical indicators; (D) correlation between (2R)-*O*-Phospho-3-sulfolactate and clinical indicators; (E) correlation between LysoPE (P-16:0/0:0) and clinical indicators.

MTB-infected macrophages inhibits *MTB* growth in the host [38].

In the present study, the levels of two kinds of LPE (LysoPE (18:1(11Z)/0:0) and LysoPE (P-16:0/0:0)) were significantly decreased in the plasma of STBs and screened as potential diagnostic biomarkers for STB. The same decrease was reported in a previous study in patients with uncomplicated pulmonary tuberculosis [39] and tuberculosis meningitis [40]. Therefore, we hypothesize that *MTB* may regulate the content of LPE by inhibiting LPE in *MTB* infection, and may inhibit the overproduction of bioactive molecules such as LTC_4, LTB_4, and 12-HETE, which further inhibits the overproduction of TNF-α, macrophage necrosis, lipid accumulation, and *MTB* growth. This ultimately reduces *MTB*-induced injury such as foamy macrophage formation, tuberculous granuloma, and caseous necrosis. Therefore, therapeutic strategies targeting the above links and MAPK [41] and GPCRs [42,43] may inhibit the reproduction and spread of *MTB* [44].

In addition, among the potential diagnostic biomarkers screened by random forest analysis, 2,3-Dinor-8-iso prostaglandin F2alpha also has high diagnostic efficacy and has been studied. 2,3-Dinor-8-iso prostaglandin F2alpha is the major metabolite of 8-iso-prostaglandin F2alpha [45], one of a large number of prostaglandins produced predominantly by free radical-catalyzed peroxidation of arachidonic acid [46]. 2,3-Dinor-8-iso prostaglandin F2alpha has been suggested as a reliable indicator of lipid peroxidation [47], which may be related to in vivo free radical generation, oxidative damage, and antioxidant deficiency [48]. As a highly infectious pathogenic bacterium, *MTB* infection causes acute oxidative stress, activation of macrophages, production of cytokines, and high levels of reactive oxygen species (ROS) [49]. Excessive inflammatory response leads to accumulation of ROS and extensive tissue and organ damage, increases ferrous iron levels associated with ferroptosis, promotes tissue damage and facilitates bacterial transmission [50,51]. In the present study, plasma levels of 2,3-Dinor-8-iso prostaglandin F2alpha were significantly increased in STBs, indicating that the organism is in a state of acute oxidative stress, which may lead to lipid peroxidation and ferroptosis, which may promote further *MTB* dissemination from cells undergoing ferroptosis.

Unfortunately, the physiological effects of the remaining three screened diagnostic markers 8-Demethyl-8-formylriboflavin 5′-phosphate [52], Glutaminyl-Gamma-glutamate [53], and (2R)-*O*-Phospho-3-sulfolactate [54] have not yet been reported and require further investigation.

Due to the limited number of samples, the STBs were not divided into pre- and post-treatment groups based on different disease courses. In this study, the peripheral blood samples of STBs were collected on the seventh day after receiving standard anti-TB drug treatment, including isoniazid (INH, 0.3 g/d), rifampicin (RIF, 0.45 g/d), pyrazinamide (PZA, 0.75 g/d), and ethambutol (EMB, 0.75 g/d). Available studies show that 50–90% of the total ingested INH is acetylated by N-acetyltransferase-2 (NAT2) to acetyl-INH (AcINH) [55,56], in addition to the formation of various hydrazones that are intermediates of the leucine and/or isoleucine, lysine, tyrosine, tryptophan, and phenylalanine metabolic pathways [57]. Approximately 85% of RIF is metabolized in the liver [58] by deacetylation via arylacetamide deacetylase to 25-deacetyl-RIF [59] or by hydrolysis to 3-formyl-RIF [60]. RIF-induced pregnane X receptor (PXR) activation inhibits CYP17A/19A and activates CYP1A/3A/7B/11B/2C [61]. PZA is deamidated to pyrazinoic acid (POA) in the liver, which is further oxidized by xanthine oxidase to 5-hydroxy-POA, or by amidase to 5-hydroxy-PZA [62]. PZA also leads to an upshift in the substrate balance in the purine pathway, and subsequently in the production of uric acid [63]. 75–80% of EMB is absorbed from the gastrointestinal tract [64] and oxidized in the liver to the intermediate aldehyde, which is then converted to a dicarboxylic acid derivative, 2,2'-(ethylenediimino)-di-butyric acid (EDBA) [65,66]. The above-mentioned metabolites and pathways of anti-TB drugs did not overlap with the five potential diagnostic biomarkers and pathways enriched in differential metabolites screened in the present study, probably because the maximum treatment period of seven days was set in the present study for all STBs included in the study, and the anti-TB drugs had not yet taken full effect to affect the metabolites, suggesting that the results of the present study were not influenced by the anti-TB drugs, but still need to be confirmed by cohort studies.

The present study has its limitations. First, no targeted metabolomic analysis to validate potential diagnostic biomarkers was performed. Second, future studies are needed to validate these findings and to analyze the association between differentially expressed metabolites and disease pathophysiology. In addition, we will continue to collect peripheral blood samples from both patients with STB and clinical patients with non-*MTB* spinal infections to validate the diagnostic biomarkers identified in this study.

5. Conclusion

Metabolites differentially expressed in STBs plasma compared to those in HCs were identified using metabolomics. Five independent diagnostic biomarkers, LysoPE (18:1(11Z)/0:0), 8-Demethyl-8-formylriboflavin 5′-phosphate, Glutaminyl-Gamma-glutamate, (2R)-*O*-Phospho-3-sulfolactate, and LysoPE (P-16:0/0:0) have good diagnostic value in distinguishing STBs from HCs. STB has important effects on lipid metabolism, particularly on the pathways involved in phospholipid metabolism, and may be involved in the pathogenesis of STB.

Ethics approval and consent to participate

All participants provided written informed consent to participate in the study. All research methods used in this study were established in accordance with the ethical guidelines of the Declaration of Helsinki and relevant regulations. All experimental protocols were approved by the Ethics Committee (full name: Medical Research Ethics Review Committee of General Hospital of Ningxia Medical University, ethical approval reference: KYLL-2021-932).

Consent for publication

Written informed consent was obtained from participants or their guardians.

Availability of data and materials

The datasets used and analyzed during the current study are available within the article and its supplementary files, or are available from the corresponding author upon reasonable request. Metabolomics data analyzed in this manuscript are available from the Mendeley Data (https://data.mendeley.com/datasets/m6dvnphgj5/1).

Funding

This work was supported by the National Natural Science Foundation of China (82260436 and 81860395), the National College Students Innovation and Entrepreneurship Training Program (202210752008), the Key Research and Development Program of Ningxia (2022BEG03099), and the 2021 First-Class Discipline Construction Founded Project of Ningxia Medical University and the School of Clinical Medicine: The application research of 3D printed personalized percutaneous guide plate in thoracolumbar puncture biopsy.

CRediT authorship contribution statement

Chaoran Wang: Writing – review & editing, Writing – original draft, Funding acquisition, Formal analysis, Data curation, Conceptualization. **Caili Lou:** Writing – review & editing, Visualization, Validation, Formal analysis, Data curation. **Zongqiang Yang:** Writing – review & editing, Methodology, Investigation, Formal analysis. **Jiandang Shi:** Writing – original draft, Methodology, Investigation, Formal analysis. **Ningkui Niu:** Writing – review & editing, Supervision, Resources, Project administration, Methodology, Funding acquisition.

Declaration of competing interest

The authors declare that they have no known competing financial interests or personal relationships that could have appeared to influence the work reported in this paper.

Acknowledgments

Not applicable.

List of abbreviations

STB	spinal tuberculosis
STBs	patients with spinal tuberculosis
HCs	healthy controls
TB	tuberculosis
MTB	*Mycobacterium tuberculosis*
DR	digital radiography
CT	computed tomography
MRI	magnetic resonance imaging
Xpert *MTB*/RIF	Xpert *Mycobacterium tuberculosis* complex and resistance to rifampin

WGS	whole-genome sequencing
NAAT	nucleic acid amplification test
UPLC-QTOF/MS	ultra-high performance liquid chromatography coupled with quadrupole time-of-flight mass spectrometry
ESR	erythrocyte sedimentation rate
CRP	C-reactive protein
ROC	receiver operating characteristic
QCs	quality control samples
ESI	electron spray ionization
OPLS-DA	orthogonal partial least square to latent discriminant analysis
VIP	variable influence on projection
FC	fold change
RSD	relative standard deviation
PCA	principal component analysis
AUC	area under the curve
LBP	lipopolysaccharide-binding protein
LPE	lysophosphatidylethanolamine
LPLs	lysophospholipids
GPCRs	G-protein-coupled receptors
MAPK	mitogen-activated protein kinases
LTC_4	leukotriene C4
LTB_4	leukotriene B4
ROS	reactive oxygen species
INH	isoniazid
RIF	rifampicin
PZA	pyrazinamide
EMB	ethambutol
NAT2	N-acetyltransferase-2
AcINH	acetylisoniazid
PXR	pregnane X receptor
POA	pyrazinoic acid
EDBA	2,2'-(ethylenediimino)-di-butyric acid

Appendix A. Supplementary data

Supplementary data to this article can be found online at https://doi.org/10.1016/j.heliyon.2024.e27940.

References

[1] T. Li, X. Yan, X. Du, F. Huang, N. Wang, N. Ni, J. Ren, Y. Zhao, Z. Jia, Extrapulmonary tuberculosis in China: a national survey, Int. J. Infect. Dis. 128 (2023) 69–77, https://doi.org/10.1016/j.ijid.2022.12.005.

[2] D.-M. Wang, Q. An, Q. Yang, Y. Liao, Y. Jian, Osteoarticular tuberculosis cases in the southwest of China: a 9-year retrospective study, Front. Med. 10 (2023) 1051620, https://doi.org/10.3389/fmed.2023.1051620.

[3] A.K. Jain, S. Rajasekaran, K.R. Jaggi, V.P. Myneedu, Tuberculosis of the spine, J Bone Jt. Surg Am. 102 (2020) 617–628, https://doi.org/10.2106/jbjs.19.00001.

[4] N. Niu, Q. Wang, J. Shi, X. Zhang, G. Geng, S. Zhou, C. Thach, F. Cheng, Z. Wang, Clinical and genomic responses to ultra-short course chemotherapy in spinal tuberculosis, Exp. Ther. Med. 13 (2017) 1681–1688, https://doi.org/10.3892/etm.2017.4170.

[5] W. Ma, W. Jin, X. He, Y. Sun, H. Yin, Z. Wang, S. Shi, Mycobacterium tuberculosis induced osteoblast dysregulation involved in bone destruction in spinal tuberculosis, Front. Cell. Infect. Microbiol. 12 (2022) 780272, https://doi.org/10.3389/fcimb.2022.780272.

[6] J. Furin, H. Cox, M. Pai, Tuberculosis, Lancet. 393 (2019) 1642–1656, https://doi.org/10.1016/s0140-6736(19)30308-3.

[7] J.Y. Lee, Diagnosis and treatment of extrapulmonary tuberculosis, Tuberc Respir Seoul 78 (2015) 47–55, https://doi.org/10.4046/trd.2015.78.2.47.

[8] R.K. Garg, D.S. Somvanshi, Spinal tuberculosis: a review, J Spinal Cord Med 34 (2011) 440–454, https://doi.org/10.1179/2045772311y.0000000023.

[9] D. Cazabon, T. Pande, S. Kik, W. Van Gemert, H. Sohn, C. Denkinger, Z.Z. Qin, B. Waning, M. Pai, Market penetration of Xpert MTB/RIF in high tuberculosis burden countries: a trend analysis from 2014 - 2016, Gates Open Res 2 (2018) 35, https://doi.org/10.12688/gatesopenres.12842.2.

[10] K. Pandya, D. Jagani, N. Singh, CRISPR-cas systems: programmable nuclease revolutionizing the molecular diagnosis, Mol. Biotechnol. (2023), https://doi.org/10.1007/s12033-023-00819-7.

[11] S. Chattopadhyay, T. Biswas, A. Banerjee, N. Chaudhury, R. Mondal, A. Nath, Diagnostic approach to extrapulmonary tuberculosis by cartridge-based nucleic acid amplification test, J. Assoc. Physicians India. 71 (2023) 11–12, https://doi.org/10.5005/japi-11001-0260.

[12] A. Batirel, H. Erdem, G. Sengoz, F. Pehlivanoglu, E. Ramosaco, S. Gülsün, R. Tekin, B. Mete, I. Balkan, D.Y. Sevgi, E. Giannitsioti, A. Fragou, S. Kaya, B. Cetin, T. Oktenoglu, A.D. Celik, B. Karaca, E.S. Horasan, M. Ulug, S. Senbayrak, S. Kaya, E. Arslanalp, R. Hasbun, S. Ates-Guler, A. Willke, S. Senol, D. Inan, E. Güclü, G. T. Ertem, M.M. Koc, M. Tasbakan, G. Ocal, S. Kocagoz, H. Kusoglu, T. Güven, A.I. Baran, B. Dede, F.Y. Karadag, H. Yilmaz, G. Aslan, D.A. Al-Gallad, S. Cesur, R. El-Sokkary, F. Sirmatel, U. Savasci, G. Karaahmetoglu, H. Vahaboglu, The course of spinal tuberculosis (Pott disease): results of the multinational, multicentre Backbone-2 study, Clin. Microbiol. Infect. 21 (2015) 1008.e9–1008.e18, https://doi.org/10.1016/j.cmi.2015.07.013.

[13] V. Kumar, D. Neradi, B. Sherry, A. Gaurav, S.S. Dhatt, Tuberculosis of the spine and drug resistance: a review article, Neurosurg. Rev. 45 (2022) 217–229, https://doi.org/10.1007/s10143-021-01595-1.

[14] S. Ray, S.K. Patel, V. Kumar, J. Damahe, S. Srivastava, Differential expression of serum/plasma proteins in various infectious diseases: specific or nonspecific signatures, Proteomics Clin Appl 8 (2014) 53–72, https://doi.org/10.1002/prca.201300074.

[15] G.J. Patti, O. Yanes, G. Siuzdak, Innovation: metabolomics: the apogee of the omics trilogy, Nat. Rev. Mol. Cell Biol. 13 (2012) 263–269, https://doi.org/10.1038/nrm3314.

[16] R.J. DeBerardinis, K.R. Keshari, Metabolic analysis as a driver for discovery, diagnosis, and therapy, Cell 185 (2022) 2678–2689, https://doi.org/10.1016/j.cell.2022.06.029.

[17] Y. Yu, X.-X. Jiang, J.-C. Li, Biomarker discovery for tuberculosis using metabolomics, Front. Mol. Biosci. 10 (2023) 1099654, https://doi.org/10.3389/fmolb.2023.1099654.

[18] W.B. Dunn, D. Broadhurst, P. Begley, E. Zelena, S. Francis-McIntyre, N. Anderson, M. Brown, J.D. Knowles, A. Halsall, J.N. Haselden, A.W. Nicholls, I.D. Wilson, D.B. Kell, R. Goodacre, Procedures for large-scale metabolic profiling of serum and plasma using gas chromatography and liquid chromatography coupled to mass spectrometry, Nat. Protoc. 6 (2011) 1060–1083, https://doi.org/10.1038/nprot.2011.335.

[19] J. Wang, T. Zhang, X. Shen, J. Liu, D. Zhao, Y. Sun, L. Wang, Y. Liu, X. Gong, Y. Liu, Z.-J. Zhu, F. Xue, Serum metabolomics for early diagnosis of esophageal squamous cell carcinoma by UHPLC-QTOF/MS, Metabolomics 12 (2016) 116, https://doi.org/10.1007/s11306-016-1050-5.

[20] D. Sivakumaran, C. Ritz, J.E. Gjøen, M. Vaz, S. Selvam, T.H.M. Ottenhoff, T.M. Doherty, S. Jenum, H.M.S. Grewal, Host blood RNA transcript and protein signatures for sputum-independent diagnostics of tuberculosis in adults, Front. Immunol. 11 (2020) 626049, https://doi.org/10.3389/fimmu.2020.626049.

[21] D. Kiran, R.J. Basaraba, Lactate metabolism and signaling in tuberculosis and cancer: a comparative review, Front. Cell. Infect. Microbiol. 11 (2021) 624607, https://doi.org/10.3389/fcimb.2021.624607.

[22] C. Lou, J. Liu, Z. Ren, J. Ji, H. Ma, H. Dong, L. Wang, X. Zhang, N. Niu, Analysis of the value of serum biomarker LBP in the diagnosis of spinal tuberculosis, Infect. Drug Resist. 15 (2022) 4915–4926, https://doi.org/10.2147/idr.S377182.

[23] F. Crick, Central dogma of molecular biology, Nature 227 (1970) 561–563, https://doi.org/10.1038/227561a0.

[24] C. Seger, L. Salzmann, After another decade: LC-MS/MS became routine in clinical diagnostics, Clin. Biochem. 82 (2020) 2–11, https://doi.org/10.1016/j.clinbiochem.2020.03.004.

[25] A. Grzelczyk, E. Gendaszewska-Darmach, Novel bioactive glycerol-based lysophospholipids: new data – new insight into their function, Biochimie 95 (2013) 667–679, https://doi.org/10.1016/j.biochi.2012.10.009.

[26] K. Makide, H. Kitamura, Y. Sato, M. Okutani, J. Aoki, Emerging lysophospholipid mediators, lysophosphatidylserine, lysophosphatidylthreonine, lysophosphatidylethanolamine and lysophosphatidylglycerol, Prostaglandins Lipid Mediat 89 (2009) 135–139, https://doi.org/10.1016/j.prostaglandins.2009.04.009.

[27] S.J. Park, K.P. Lee, S. Kang, H.Y. Chung, Y.S. Bae, F. Okajima, D.S. Im, Lysophosphatidylethanolamine utilizes LPA(1) and CD97 in MDA-MB-231 breast cancer cells, Cell. Signal. 25 (2013) 2147–2154, https://doi.org/10.1016/j.cellsig.2013.07.001.

[28] K.S. Park, H.Y. Lee, S.Y. Lee, M.K. Kim, S.D. Kim, J.M. Kim, J. Yun, D.S. Im, Y.S. Bae, Lysophosphatidylethanolamine stimulates chemotactic migration and cellular invasion in SK-OV3 human ovarian cancer cells: involvement of pertussis toxin-sensitive G-protein coupled receptor, FEBS Lett. 581 (2007) 4411–4416, https://doi.org/10.1016/j.febslet.2007.08.014.

[29] A. Nishina, H. Kimura, A. Sekiguchi, R.H. Fukumoto, S. Nakajima, S. Furukawa, Lysophosphatidylethanolamine in Grifola frondosa as a neurotrophic activator via activation of MAPK, J. Lipid Res. 47 (2006) 1434–1443, https://doi.org/10.1194/jlr.M600045-JLR200.

[30] J.M. Lee, S.J. Park, D.S. Im, Lysophosphatidylethanolamine increases intracellular Ca(2+) through LPA(1) in PC-12 neuronal cells, Biochem. Biophys. Res. Commun. 461 (2015) 378–382, https://doi.org/10.1016/j.bbrc.2015.04.042.

[31] N.D. Hung, M.R. Kim, D.E. Sok, 2-Polyunsaturated acyl lysophosphatidylethanolamine attenuates inflammatory response in zymosan A-induced peritonitis in mice, Lipids 46 (2011) 893–906, https://doi.org/10.1007/s11745-011-3589-2.

[32] E. Pace, M. Profita, M. Melis, A. Bonanno, A. Paternò, C.H. Mody, M. Spatafora, M. Ferraro, L. Siena, A.M. Vignola, G. Bonsignore, M. Gjomarkaj, LTB4 is present in exudative pleural effusions and contributes actively to neutrophil recruitment in the inflamed pleural space, Clin. Exp. Immunol. 135 (2004) 519–527, https://doi.org/10.1111/j.1365-2249.2003.02387.x.

[33] O. el-Ahmady, M. Mansour, H. Zoeir, O. Mansour, Elevated concentrations of interleukins and leukotriene in response to Mycobacterium tuberculosis infection, Ann. Clin. Biochem. 34 (Pt 2) (1997) 160–164, https://doi.org/10.1177/000456329703400205.

[34] K.G. Nore, M.J. Jørgensen, A.M. Dyrhol-Riise, S. Jenum, K. Tonby, Elevated levels of anti-inflammatory eicosanoids and monocyte heterogeneity in Mycobacterium tuberculosis infection and disease, Front. Immunol. 11 (2020) 579849, https://doi.org/10.3389/fimmu.2020.579849.

[35] S.K. Lau, K.C. Lee, S.O. Curreem, W.N. Chow, K.K. To, I.F. Hung, D.T. Ho, S. Sridhar, I.W. Li, V.S. Ding, E.W. Koo, C.F. Wong, S. Tam, C.W. Lam, K.Y. Yuen, P. C. Woo, Metabolomic profiling of plasma from patients with tuberculosis by use of untargeted mass spectrometry reveals novel biomarkers for diagnosis, J. Clin. Microbiol. 53 (2015) 3750–3759, https://doi.org/10.1128/jcm.01568-15.

[36] D.M. Tobin, J.C. Vary Jr., J.P. Ray, G.S. Walsh, S.J. Dunstan, N.D. Bang, D.A. Hagge, S. Khadge, M.C. King, T.R. Hawn, C.B. Moens, L. Ramakrishnan, The lta4h locus modulates susceptibility to mycobacterial infection in zebrafish and humans, Cell 140 (2010) 717–730, https://doi.org/10.1016/j.cell.2010.02.013.

[37] D.M. Tobin, F.J. Roca, J.P. Ray, D.C. Ko, L. Ramakrishnan, An enzyme that inactivates the inflammatory mediator leukotriene b4 restricts mycobacterial infection, PLoS One 8 (2013) e67828, https://doi.org/10.1371/journal.pone.0067828.

[38] H. Salamon, N. Bruiners, K. Lakehal, L. Shi, J. Ravi, K.D. Yamaguchi, R. Pine, M.L. Gennaro, Cutting edge: vitamin D regulates lipid metabolism in Mycobacterium tuberculosis infection, J. Immunol. 193 (2014) 30–34, https://doi.org/10.4049/jimmunol.1400736.

[39] J.X. Chen, Y.S. Han, S.Q. Zhang, Z.B. Li, J. Chen, W.J. Yi, H. Huang, T.T. Jiang, J.C. Li, Novel therapeutic evaluation biomarkers of lipid metabolism targets in uncomplicated pulmonary tuberculosis patients, Signal Transduct Target Ther 6 (2021) 22, https://doi.org/10.1038/s41392-020-00427-w.

[40] J. Wang, Q. Zhao, G. Feng, Q. Zhu, W. Wang, T. Bian, G. Zhao, [Leukotriene B4 level in cerebrospinal fluid of patients with tuberculosis meningitis and clinical significance], Xi Bao yu fen zi mian yi xue, Za Zhi 31 (2015) 1108–1111.

[41] M. Arish, F. Naz, Macrophage plasticity as a therapeutic target in tuberculosis, Eur. J. Immunol. 52 (2022) 696–704, https://doi.org/10.1002/eji.202149624.

[42] P.T. Elkington, J.E. Emerson, L.D. Lopez-Pascua, C.M. O'Kane, D.E. Horncastle, J.J. Boyle, J.S. Friedland, Mycobacterium tuberculosis up-regulates matrix metalloproteinase-1 secretion from human airway epithelial cells via a p38 MAPK switch, J. Immunol. 175 (2005) 5333–5340, https://doi.org/10.4049/jimmunol.175.8.5333.

[43] L. Monin, S.A. Khader, Chemokines in tuberculosis: the good, the bad and the ugly, Semin. Immunol. 26 (2014) 552–558, https://doi.org/10.1016/j.smim.2014.09.004.

[44] F. Naz, M. Arish, GPCRs as an emerging host-directed therapeutic target against mycobacterial infection: from notion to reality, Br. J. Pharmacol. 179 (2022) 4899–4909, https://doi.org/10.1111/bph.15315.

[45] L.J. Roberts, K.P. Moore, W.E. Zackert, J.A. Oates, J.D. Morrow, Identification of the major urinary metabolite of the F2-isoprostane 8-iso-prostaglandin F2alpha in humans, J. Biol. Chem. 271 (1996) 20617–20620, https://doi.org/10.1074/jbc.271.34.20617.

[46] J.D. Morrow, K.E. Hill, R.F. Burk, T.M. Nammour, K.F. Badr, L.J. Roberts, A series of prostaglandin F2-like compounds are produced in vivo in humans by a non-cyclooxygenase, free radical-catalyzed mechanism, Proc. Natl. Acad. Sci. U. S. A. 87 (1990) 9383–9387, https://doi.org/10.1073/pnas.87.23.9383.

[47] C. Chiabrando, A. Valagussa, C. Rivalta, T. Durand, A. Guy, E. Zuccato, P. Villa, J.C. Rossi, R. Fanelli, Identification and measurement of endogenous beta-oxidation metabolites of 8-epi-Prostaglandin F2alpha, J. Biol. Chem. 274 (1999) 1313–1319, https://doi.org/10.1074/jbc.274.3.1313.

[48] Y. Liang, P. Wei, R.W. Duke, P.D. Reaven, S.M. Harman, R.G. Cutler, C.B. Heward, Quantification of 8-iso-prostaglandin-F2α and 2,3-dinor-8-iso-prostaglandin-F2α in human urine using liquid chromatography-tandem mass spectrometry, Free Radic. Biol. Med. 34 (2003) 409–418, https://doi.org/10.1016/S0891-5849(02)01018-3.

[49] K.C. Chinta, M.A. Rahman, V. Saini, J.N. Glasgow, V.P. Reddy, J.M. Lever, S. Nhamoyebonde, A. Leslie, R.M. Wells, A. Traylor, R. Madansein, G.P. Siegal, V. B. Antony, J. Deshane, G. Wells, K. Nargan, J.F. George, P.K. Ramdial, A. Agarwal, A.J.C. Steyn, Microanatomic distribution of myeloid heme oxygenase-1 protects against free radical-mediated immunopathology in human tuberculosis, Cell Rep. 25 (2018) 1938–1952, https://doi.org/10.1016/j.celrep.2018.10.073, e5.

[50] E.P. Amaral, D.L. Costa, S. Namasivayam, N. Riteau, O. Kamenyeva, L. Mittereder, K.D. Mayer-Barber, B.B. Andrade, A. Sher, A major role for ferroptosis in Mycobacterium tuberculosis-induced cell death and tissue necrosis, J. Exp. Med. 216 (2019) 556–570, https://doi.org/10.1084/jem.20181776.

[51] S. Yang, J. Ouyang, Y. Lu, V. Harypursat, Y. Chen, A dual role of heme oxygenase-1 in tuberculosis, Front. Immunol. 13 (2022) 842858, https://doi.org/10.3389/fimmu.2022.842858.
[52] PubChem, 8-Demethyl-8-formylriboflavin 5'-phosphate, (n.d). https://pubchem.ncbi.nlm.nih.gov/compound/126961147 (accessed July 22, 2023).
[53] PubChem, Glutaminyl-Gamma-glutamate, (n.d). https://pubchem.ncbi.nlm.nih.gov/compound/131750740 (accessed July 22, 2023).
[54] PubChem, (2R)-O-Phospho-3-sulfolactate, (n.d.). https://pubchem.ncbi.nlm.nih.gov/substance/13703 (accessed July 22, 2023).
[55] D.J. Klein, S. Boukouvala, E.M. McDonagh, S.R. Shuldiner, N. Laurieri, C.F. Thorn, R.B. Altman, T.E. Klein, PharmGKB summary: isoniazid pathway, pharmacokinetics, Pharmacogenet. Genomics. 26 (2016) 436–444, https://doi.org/10.1097/FPC.0000000000000232.
[56] P. Wang, K. Pradhan, X.-B. Zhong, X. Ma, Isoniazid metabolism and hepatotoxicity, Acta Pharm. Sin. B 6 (2016) 384–392, https://doi.org/10.1016/j.apsb.2016.07.014.
[57] F. Li, Y. Miao, L. Zhang, S.A. Neuenswander, J.T. Douglas, X. Ma, Metabolomic analysis reveals novel isoniazid metabolites and hydrazones in human urine, Drug Metab. Pharmacokinet. 26 (2011) 569–576, https://doi.org/10.2133/dmpk.DMPK-11-RG-055.
[58] M.A. Arbex, M. de C.L. Varella, H.R. de Siqueira, F.A.F. de Mello, Antituberculosis drugs: drug interactions, adverse effects, and use in special situations. Part 1: first-line drugs, J. Bras. Pneumol. Publicacao Of. Soc. Bras. Pneumol. E Tisilogia. 36 (2010) 626–640, https://doi.org/10.1590/s1806-37132010000500016.
[59] A. Nakajima, T. Fukami, Y. Kobayashi, A. Watanabe, M. Nakajima, T. Yokoi, Human arylacetamide deacetylase is responsible for deacetylation of rifamycins: rifampicin, rifabutin, and rifapentine, Biochem. Pharmacol. 82 (2011) 1747–1756, https://doi.org/10.1016/j.bcp.2011.08.003.
[60] V. Ramappa, G.P. Aithal, Hepatotoxicity related to anti-tuberculosis drugs: Mechanisms and management, J. Clin. Exp. Hepatol. 3 (2013) 37–49, https://doi.org/10.1016/j.jceh.2012.12.001.
[61] B. Kim, J.-Y. Moon, M.H. Choi, H.H. Yang, S. Lee, K.S. Lim, S.H. Yoon, K.-S. Yu, I.-J. Jang, J.-Y. Cho, Global metabolomics and targeted steroid profiling reveal that rifampin, a strong human PXR activator, alters endogenous urinary steroid markers, J. Proteome Res. 12 (2013) 1359–1368, https://doi.org/10.1021/pr301021p.
[62] J.J. Saukkonen, D.L. Cohn, R.M. Jasmer, S. Schenker, J.A. Jereb, C.M. Nolan, C.A. Peloquin, F.M. Gordin, D. Nunes, D.B. Strader, J. Bernardo, R. Venkataramanan, T.R. Sterling, ATS (American thoracic society) hepatotoxicity of antituberculosis therapy subcommittee, an official ATS statement: hepatotoxicity of antituberculosis therapy, Am. J. Respir. Crit. Care Med. 174 (2006) 935–952, https://doi.org/10.1164/rccm.200510-1666ST.
[63] A. Bugrim, T. Nikolskaya, Y. Nikolsky, Early prediction of drug metabolism and toxicity: systems biology approach and modeling, Drug Discov. Today 9 (2004) 127–135, https://doi.org/10.1016/S1359-6446(03)02971-4.
[64] S. Sarkar, A. Ganguly, Current overview of anti-tuberculosis drugs: metabolism and toxicities, Mycobact. Dis. 6 (2016), https://doi.org/10.4172/2161-1068.1000209.
[65] M.A. Arbex, M. de C.L. Varella, H.R. de Siqueira, F.A.F. de Mello, Antituberculosis drugs: drug interactions, adverse effects, and use in special situations. Part 1: first-line drugs, J. Bras. Pneumol. Publicacao Of. Soc. Bras. Pneumol. E Tisilogia. 36 (2010) 626–640, https://doi.org/10.1590/s1806-37132010000500016.
[66] C. Becker, J.B. Dressman, G.L. Amidon, H.E. Junginger, S. Kopp, K.K. Midha, V.P. Shah, S. Stavchansky, D.M. Barends, Biowaiver monographs for immediate release solid oral dosage forms: ethambutol dihydrochloride, J. Pharm. Sci. 97 (2008) 1350–1360, https://doi.org/10.1002/jps.21061.